Geophys. J. Int. (2009) **176,** 1–13 doi: 10.1111/j.1365-246X.2008.03818.x

Response of the ionosphere to the seismic trigerred acoustic waves: electron density and electromagnetic fluctuations

E. Alam Kherani,[1,2] Philippe Lognonné,[1] Nishant Kamath,[1] Francois Crespon[1,3] and R. Garcia[1,4]

Equipe Géophysique Spatiale et Planétologie, IPGP, UMR 7154-CNRS- *Paris Diderot,* 4 *Avenue de Neptune,* 94100, *Saint Maur des Fossés, Paris. E-mail: alam@ipgp.jussieu.fr*
[2]*Institute de Nacional Pesquisais Espaciais, São José dos Campos, Brasil*
[3]*NOVELTIS, Parc Technologique du Canal,* 2, *Avenue de l Europe* 31520 *Ramonville Sainte-Agne, France*
[4]*Dynamique Terrestre et Planétaire, Observatoire Midi-Pyrénées - Université Toulouse* 3, 14, *ave E. Belin,* 31400 *Toulouse, France*

Accepted 2008 April 10. Received 2008 January 12; in original form 2007 April 29

SUMMARY

We study the excitation of low-frequency (0.001–10 Hz) electromagnetic and density fluctuations in the ionosphere during the passage of seismic triggered acoustic waves (AWs). The study involves the generation of ionospheric currents by AWs and subsequent perturbations of the electromagnetic fields and ion and electron density. In this study, the non-local analysis of the fluctuations is carried out in the framework of hydromagnetic theory. Our objective is to examine the spatial and frequency distributions of these fluctuations and to compare them qualitatively with the available observations. The dynamics of both electrojet and F region of ionosphere are included. Also included are the effects of the dip-angle variations of the Earth's magnetic field. Significant anisotropy and inhomogeneities are noted in the fluctuations. The amplitudes of current and magnetic field fluctuations are found to be maximum in the F region where ion inertia is large enough to support the plasma waves and where electron number density and acoustic wave amplitudes are also large. The density fluctuations also follow similar trends. Both electromagnetic and density fluctuations are large in the latitude region where the acoustic wave vibration parallel to the Earth's magnetic field is large. The fluctuations have the tendency to be maximum in the 0.1–1 Hz frequency range. In this range, AWs driven currents and electromagnetic fluctuations may become of order of μAm^{-2}, $nV\,m^{-1}$ and nT, respectively in the F region.

Key words: Ionosphere/atmosphere interactions; Earthquake dynamics.

1 INTRODUCTION

Ionosphere is a part of Earth's atmosphere above 80 km which is significantly ionized and has, therefore, free ions and electrons. It mainly consists of two conducting layers known as E (80–130 km) and F layer (above 180 km). During the seismic activity, varieties of signatures are observed in these layers. These include the fluctuations in the ionospheric density or total electron content (TEC), height of the ionospheric layer and the electromagnetic fields (Yuen *et al.* 1969; Chmyrev *et al.* 1989; Lognonné *et al.* 2006, for a review of the TEC observations). These disturbances are detected from the dense GPS network and found to be associated with the acoustic-gravity (AGWs), seismic and Tsunami waves (Calais & Minster 1995; Afraimovich *et al.* 2001; Ducic *et al.* 2003; Artru *et al.* 2004; Hobara & Parrot 2005; DasGupta *et al.* 2006; Hao *et al.* 2006; Liu *et al.* 2006a). Signals are also detected with other techniques, such as the TEC measurements from the altimetric radars (Occhipinti *et al.* 2006) and ionospheric velocities measurements by Doppler HF radar (Artru *et al.* 2001, 2004, 2005; Liu *et al.* 2006b).

These observations indicate the existence of energy flow mechanisms from the lithosphere to the ionosphere. The coupling through AGWs is found to be quite effective (Lognonné *et al.* 1998; Koshevaya *et al.* 2005) due to their excitation by the displacements of the terrestrial surface and their large amplitudes at ionospheric heights (Ahmadov & Kunitsyn 2004). Lognonné *et al.* (1998) have shown that a fraction of about 10^{-6} of the seismic energy is injected in the atmosphere for frequency larger than 5 mHz via this channel. Moreover, at certain frequencies such as about 3.7 and 4.4 mHz, energy escape to the atmosphere is found to be an order of magnitude large. In the ionosphere, this channel should manifest in different phenomena, such as, the plasma wave excitation, linear and non-linear generations of electro-magnetic fluctuations and the oscillations of E and F-layers (Aburjania & Machabeli 1997; Occhipinti *et al.* 2006).

In this work, the excitation of ionospheric low-frequency electromagnetic and density fluctuations by acoustic waves is studied in the framework of hydromagnetic theory. This problem has been pursued in the past (Jacobson & Bernhardt 1985; Borisov & Moiseyev 1989; Surukov 1992; Pokhotelov *et al.* 1995; Aburjania & Machabeli 1997; Sorokin *et al.* 2006). However, these investigations are either confined to the E region where the large equatorial electrojet current (EEJ) flows in the presence of Cowling conductivity (Kelley 1989) or to the particular latitude with assumption of either vertical or horizontal terrestrial magnetic field.

Indeed, presence of large Cowling conductivity makes the E region a preferential location for searching any kind of electromagnetic fluctuations. On the other hand, the wind amplitude associated with the seismic triggered AGWs, that drives the currents in the present scenario, remains small in the E region. It becomes large only in the F region where electron number density is also large. Thus a large current is expected to flow in this region. The importance of F region in the excitation of AWs induced fluctuations was first pointed out by Woo & Kahalas (1970). Their 1-D non-local analysis revealed the coupling between AWs and ionosphere to be maximum in the F region. They had also found this coupling to be maximum in the 0.1–1 Hz frequency range. Their study, however, did not include the effects of Earth's magnetic field. More recently, Rapoport *et al.* (2004) have investigated the linear-local effects of AGWs in the ionosphere and found the maximum response in the F region. The non-linear 3-D simulation of Sumatra tsunami (2004 December 26, epicentre: 3.3°N, 95.8°E, $M \sim 9.3$, depth ~30 km) also reveals similar features (Occhipinti *et al.* 2006, 2008). This confirms previous TEC observations after other large quakes (Naaman *et al.* 2001; Ducic *et al.* 2003; Garcia *et al.* 2005a), and indicates that the maximum density perturbations generated by seismic waves to be in the F region. It is therefore, essential to include the F region dynamics in the investigation. Furthermore, knowing that the ionospheric conductivities have strong anisotropic nature with respect to the ambient magnetic field a realistic field geometry is requested.

Our objective in this study to examine the non-local behavior of the excitation of electromagnetic and density fluctuations in the ionosphere, to compare their relative magnitudes in the E and F region and to study their variations with respect to the dip-angle of Earth's magnetic field and frequency of AWs. The set of hydromagnetic equations, described in Section 2, are solved numerically for this purpose. The results are discussed in Section 3.

2 NON-LOCAL ANALYSIS

The terrestrial ionosphere is a weakly ionized plasma where inertia of the atmosphere is much larger than the inertia of the ionized medium. The momentum transfer from neutrals to the ionosphere is effectively instantaneous while the transfer from ionosphere to atmosphere takes more than 2 hr (Kelley 1989). Thus, the atmospheric waves such as the AWs can be seen as the forcing or driving source whose characteristics remain undisturbed by the ionospheric perturbation, even in the extreme low frequency range. To study the excitation of fluctuations in the ionosphere caused by such neutral wave, we start from the momentum, continuity, Maxwell (in wave from, see Parks 2004) and Ohm's law equations, respectively written as:

$$\frac{\mathrm{d}\vec{u_s}}{\mathrm{d}t} = -c_s^2 \nabla \log n_s + \frac{q_s}{m_s}(\vec{E} + \vec{u}_s \times \vec{B}) - \nu_s \vec{u}_s + \nu_s \vec{W} + \vec{g}, \quad (1)$$

$$\frac{\partial n_s}{\partial t} + \nabla.(n_s \vec{u_s}) = P_s, \quad (2)$$

$$\vec{J}^W = \sum_s q_s n_s \vec{u}_s \quad (3)$$

$$\nabla^2 \vec{E} - \nabla(\nabla.\vec{E}) - \frac{1}{c^2}\frac{\partial^2 \vec{E}}{\partial t^2} - \mu_o \frac{\partial \vec{J}}{\partial t} = 0, \quad (4)$$

$$\nabla^2 \vec{B} - \frac{1}{c^2}\frac{\partial^2 \vec{B}}{\partial t^2} = -\mu_o \nabla \times \vec{J}, \quad (5)$$

$$\vec{J} = \underline{\sigma}.\vec{E} + \vec{J}^W, \quad (6)$$

where $(n_s,\ \vec{u_s})$ are the number density, velocity of plasma fluid 's' [s = ions(i)/electrons(e)], $(q_{i,e} = +Z_i e, -e)$, $(\vec{W}, \vec{g})$ are the amplitudes of AWs and weight acceleration, respectively, ν_s is the frequency of collision between species s-to neutral, $\vec{B}$ is the Earth's magnetic field and $\vec{J^W}$ is the ionospheric current density caused by mechanical forces such as the AWs and pressure gradient. $(\vec{E},\ \vec{J},\ \vec{B})$ in above equations are the fluctuating electric field, net current and magnetic field in the ionosphere, $\underline{\sigma}$ is the ionospheric conductivity tensor and $(c_s = \sqrt{\frac{kT_s}{m_s}},\ c = \frac{1}{\sqrt{\mu_o \epsilon_o}})$ are the thermal velocity of species 's' and the speed of light, respectively. Here (T_s, m_s) are the temperature and mass of the ionospheric species 's' and $(\mu_o, \epsilon_o)$are the magnetic susceptibility and dielectric permittivity in the vacuum. P_s are the production and loss of ions and electrons by photoionization and chemical reactions. We assume temperature of ions and electrons to be the same as the temperature of neutral particles in the atmosphere.

In addition to wave eq. (4), $\vec{E}$ also satisfies the charge neutrality condition given by following equation:

$$\nabla.\vec{J} = 0 \text{ or } \nabla.(\sigma.\vec{E} + \vec{J}^W) = 0 \quad (7)$$

Taking the divergence of wave eq. (4) and using above condition and vector identity, $\nabla(\nabla.\vec{E}) = \nabla^2\vec{E} - \nabla \times \nabla \times \vec{E}$, the following equation is obtained:

$$\nabla.\left[\frac{1}{c^2}\frac{\partial^2 E}{\partial t^2}\right] = 0 \ \Rightarrow \nabla.\vec{E} = 0 \quad (8)$$

which is the Gauss equation under charge neutrality condition, used to eliminate $\nabla.\vec{E}$ in (4).

In this paper, we look for linearized solutions which can be expressed as:

$$\zeta(\vec{r}, t) = \zeta_0(\vec{r}, t) + \delta\zeta(\vec{r}, t) = \zeta_0(\vec{r}, t) + \int \delta\zeta(\vec{r}, \omega) e^{-i\omega t}\, \mathrm{d}\omega,$$

where $\delta\zeta$ is the first-order perturbation (in time or in Fourier domain) over the steady state ζ_o and ω is the angular frequency of the fluctuations. The steady state ionosphere is described as the stable equilibrium state without acoustic winds (i.e. $\delta\vec{W} = 0$). The gravity term in (1) is larger than the wind term above 400 km altitude where ν_s is less than 0.1 s^{-1}. In this equlibrium state, the gravity is generally balanced by the pressure force and equilibrium electric field in the ionosphere. We will later assume that the gravity is not perturbed and that the gravity perturbation associated to the low frequency modes can be ignored here. Both the steady state wind, the gravity and the equilibrium pressure force will disappear in the linearized perturbed equation. Let us focus on the perturbations and neglect the time dependence of the steady state during the waves

propagation period. The above hydromagnetic equations then reduce to the following Fourier forms:

$$i\omega\delta\vec{u}_s + \vec{u}_{0s}.\nabla\delta\vec{u}_s = -c_s^2\frac{\nabla\delta n}{n_o} + \frac{q_s}{m_s}[\delta\vec{E} + \delta\vec{u}_s \times \vec{B_o} + \vec{u}_{0s} \times \delta\vec{B}] - \nu_s\delta\vec{u}_s + \nu_s\delta\vec{W} \quad (9)$$

$$i\omega\delta n = -\nabla.(n_o\delta\vec{u}_s) - \nabla.(\delta n\vec{u}_{0s}) + \delta P_s \quad (10)$$

$$\nabla^2\delta\vec{E} + \frac{\omega^2}{c^2}\delta\vec{E} = i\omega\mu_o\vec{\delta J} \quad (11)$$

$$\nabla^2\delta\vec{B} + \frac{\omega^2}{c^2}\delta\vec{B} = -\mu_o\nabla\times\delta\vec{J}. \quad (12)$$

We will assume in the following that sound speed ($500 < c_a < 1000\,\mathrm{m\,s^{-1}}$) of the high altitude neutral atmosphere is large with respect to the steady flow typical velocities and that the advection term in (9) can, therefore, be neglected. Maxwell equations shows also that $\delta E \simeq c_a\delta B$ and under the same approximation, the magnetic field perturbation term in (9) can be neglected with respect to the electric field perturbation term. Eq. (9) can then be rewritten as:

$$[i\omega + \nu_s]\delta\vec{u}_s - \frac{q_s}{m_s}\delta\vec{u}_s \times \vec{B_o} = -c_s^2\frac{\vec{\nabla}\delta n}{n_o} + \frac{q_s}{m_s}\delta\vec{E} + \nu_s\delta\vec{W}$$

leading, therefore, to

$$\vec{\delta u}_s = \frac{q_s}{m_s\nu_s}\underline{\varrho}_s.\delta\vec{E} + \underline{\varrho}_s.\delta\vec{W} - \frac{c_s^2}{\nu_s n_o}\underline{\varrho}_s.\vec{\nabla}\delta n \quad (9a)$$

where $\underline{\varrho}_s$ is the mobility tensor described in Appendix A. For the continuity eq. (10), we will assume that the waves do not generate changes in the production processes and that $\delta P_s = 0$. With the same assumption as above, we can rewrite eq. (10):

$$i\omega\delta n - \nabla.\left(\underline{\varrho}_s.\frac{c_s^2}{\nu_s}\nabla\delta n\right) = -\nabla.\left[n_o\underline{\varrho}_s.\left(\delta\vec{W} + \frac{q_s}{m_s\nu_s}\delta\vec{E}\right)\right] \quad (10a)$$

In (11) and (12), total current density, $\delta\vec{J}$, is given by:

$$\delta\vec{J} = \underline{\sigma}.\delta\vec{E} + \vec{J}^W = \underline{\sigma}.\delta\vec{E} + \sum_s Z_s\left[n_{0s}\delta\vec{u}_s + \delta n_s\vec{u'}_{0s}\right] \simeq \underline{\sigma}.\delta\vec{E} + \sum_s Z_s n_{0s}\delta\vec{u}_s; \quad (13)$$

and where $\underline{\sigma}$ is the conductivity tensor described in Appendix A. $\vec{u'}_{0s}$ is the steady flow related to mechanical forces (eg. TIDs) and is neglected here with respect to the other term. Eqs (9a)–(10a) and (11)–(13) form the closed set of equations for this problem. These equations are solved numerically using the finite difference successive-overrelaxation method. This algorithm was recently used by Alam *et al.* (2004, 2005) and Occhipinti *et al.* (2006) to solve the Poisson and continuity equations in the ionosphere. At first, (10a) is solved for δn assuming a null electric field perturbation. The $\delta\vec{u}$ is then obtained from (9a), again assuming a null electric field perturbation. These first iteration solutions are subsequently used to calculate $\vec{J}^W$ in (13). Eqs (11) and (12) are then solved for $\delta\vec{E}$ and $\delta\vec{B}$, and iterations are done for δn and $\delta\vec{u}$ with (10a)–(9a).

In this investigation, a 3-D ionosphere is considered. It is extended from 90 to 600 km in altitude, -45° to 45° in the geomagnetic latitude and 71–101° in the longitude. We note that the current continuity or closure is ensured everywhere in the simulation volume since eq. (7) is self-consistently included in the calculation. In addition, all boundaries are assumed to be transmitive so that the gradients in all the ambient parameters vanish at these boundaries. The radial components of δE and δB are continuous across the lower and upper boundaries since $\nabla.\delta B = \nabla.\delta E = 0$ everywhere. In addition, at these boundaries, the electron density of ionosphere is insignificant and thus the current density and conductivity are assumed to vanish there. Thus the δE and δB outside these boundaries satisfy the Laplace equation for low frequency electromagnetic waves. The derivatives of (δE, δB) and their tangential components at the boundaries are derived by equating the wave eqs (11) and (12) and corresponding Laplace equations at the boundaries and let then the thickness of boundaries approaching to zero (Sorokin *et al.* 2006).

3 RESULTS AND DISCUSSION

3.1 Atmospheric and Ionospheric parameters and amplitude of AWs

In Appendix A, the mobility and conductivity tensors appearing in (9a, 10a and 13) are derived using (9). These tensors depend on various atmospheric and ionospheric parameters such as the collision frequencies, gyrofrequencies or Earth's magnetic field and the ions and electron densities in the ionosphere. In this investigation, these parameters are determined from the MSIS (Hedin 1987), IRI (Bilitza 2001) and SAMI2 (Huba *et al.* 2000) models. The atmospheric neutral density and temperature, derived from MSIS model, are plotted in Figs 1(a) and (b). The ion-neutral and electron-neutral collision frequencies, derived from SAMI2 model, are plotted in Fig. 1(c). The ionospheric electron density, derived from the IRI, is plotted in Fig. 1(d) for an early morning hour condition (5 a.m. at 101° longitude). The vectors in this plot represent the Earth's magnetic field which is obtained from the IGRF model. In this figure, density variation with respect to latitude–altitude is shown at a particular longitude (101° east). The same scheme of representation is adopted in Figs 3 and 4 also.

The amplitude, $\delta\vec{W}$, of AWs appearing in the eq. (9) is estimated using the wave-propagation model (Garcia *et al.* 2005b). The model solves the Fourier transformed 1-D (vertical) acoustic wave equation for a given ground displacement and frequency. The assumption of vertical propagation of AWs is justified because the acoustic rays reaching ionospheric heights must have incident angles at the ground lower than 6 degrees due to the atmospheric sound velocity profile and also because the vertical wavenumber is much larger than the horizontal wavenumber. The wind amplitude, $\delta\vec{W}$, is estimated for 5 mHz frequency and assuming a 1 mm ground displacement. The 1 mm is a typical value of the surface wave amplitude of $M \sim 8$ quake worldwide. A 1 mm displacement at 5 mHz generates δW of about $2 \times 10^{-5}\,\mathrm{m\,s^{-1}}$ at the ground. It will be amplified with altitude, y, by factor $\sqrt{\frac{\rho_{\mathrm{ground}}=\rho(0)}{\rho(y)}}$ due to the exponentially decreasing mass density ρ of the neutral atmosphere. This amplification results from the fact that at long periods longer than 20 s, the viscous losses are small and the kinetic energy of the wave is then conservated (Artru *et al.* 2001). The wave amplitude should, therefore, increase with the altitude as the density of the atmosphere decreases (Hines 1960). The amplification factor and wind δW are shown in Fig. 2(a). The wind reaches the maximum $5\,\mathrm{m\,s^{-1}}$ amplitude at around 400 km and then decreases again due to the viscosity and thermal conductivity. In reality, the vertical displacement caused by the seismic waves varies significantly over the Earth's surface (Lognonné *et al.* 1998) and the uniform displacement taken in this study is not realistic. To compare the theory with the observations of particular seismic event, determination of realistic distribution of surface displacement

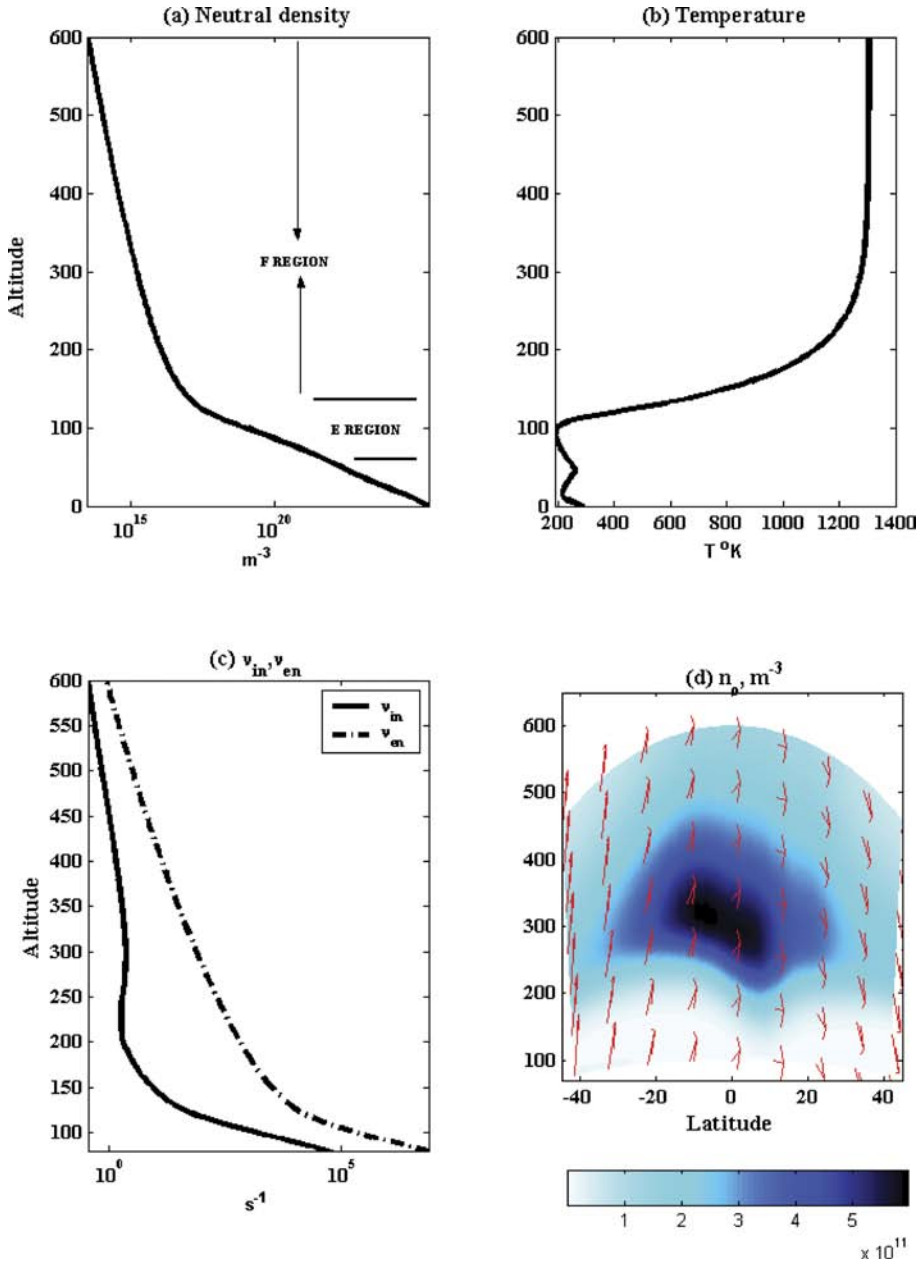

Figure 1. The altitude variations of (a) neutral density, (b) ion/electron temperature, (c) ion-neutral/electron-neutral collision frequencies and (d) The latitude–altitude distribution of the (a) electron number density n_o.

will be necessary, easily done by seismogram modelling techniques (Lognonné & Clévédé 2002; Clévédé & Lognonné 2003).

This assumption is however a choice of the authors, as we want to focus our paper to the neutral/atmosphere coupling effects and on the estimation of the ionospheric fluctuations and their variations with respect to the AWs frequency and dip-angle of Earth's magnetic field, in both the E and F region.

3.2 AWs driven current ($\vec{J}^W$) in the Ionosphere

In (9) the terms appearing with frequencies ω and ν_s correspond to the inertia (IIA) and dynamo (DIA) induced accelerations, respectively. Their comparative role to determine the ionospheric fluctuations is related to the ratio $\eta_{i,e} = i\omega/\nu_{i,e}$ appearing in the mobility tensor in Appendix A. For wave of a few mHz frequency, this ratio is much smaller than unity in the E and lower F region and becomes comparable to unity above 450 km due to decreasing ν_s with altitude. Thus, the DIA dominates in the E and lower F region whereas the IIA becomes important in the F region. In order to understand this aspect quantitatively, the altitude variation of three components $J^W_{r,\theta,\phi}$ of current $\vec{J}^W$ are plotted in Figs 2(b) and (c) without the ω term (i.e. $\eta_{i,e} = 0$ in A1) and with ω term (i.e. $\eta_{i,e} \neq 0$ in A1), respectively. In these plots, the components are summed over latitude and longitude. Also the uniform-isotropic $\delta W_{r,\theta,\phi} = 5\ \mathrm{m\,s^{-1}}$ is assumed in order to study the effect of altitude variation of $\eta_{i,e}$. The two maxima in the perturbed current is seen in the plots, first in the electrojet (EJ) region near 105 km altitude and second in the F region. In the E region, all the three components of J^W are unaltered with and without IIA term in (9). On the other hand, in the F region,

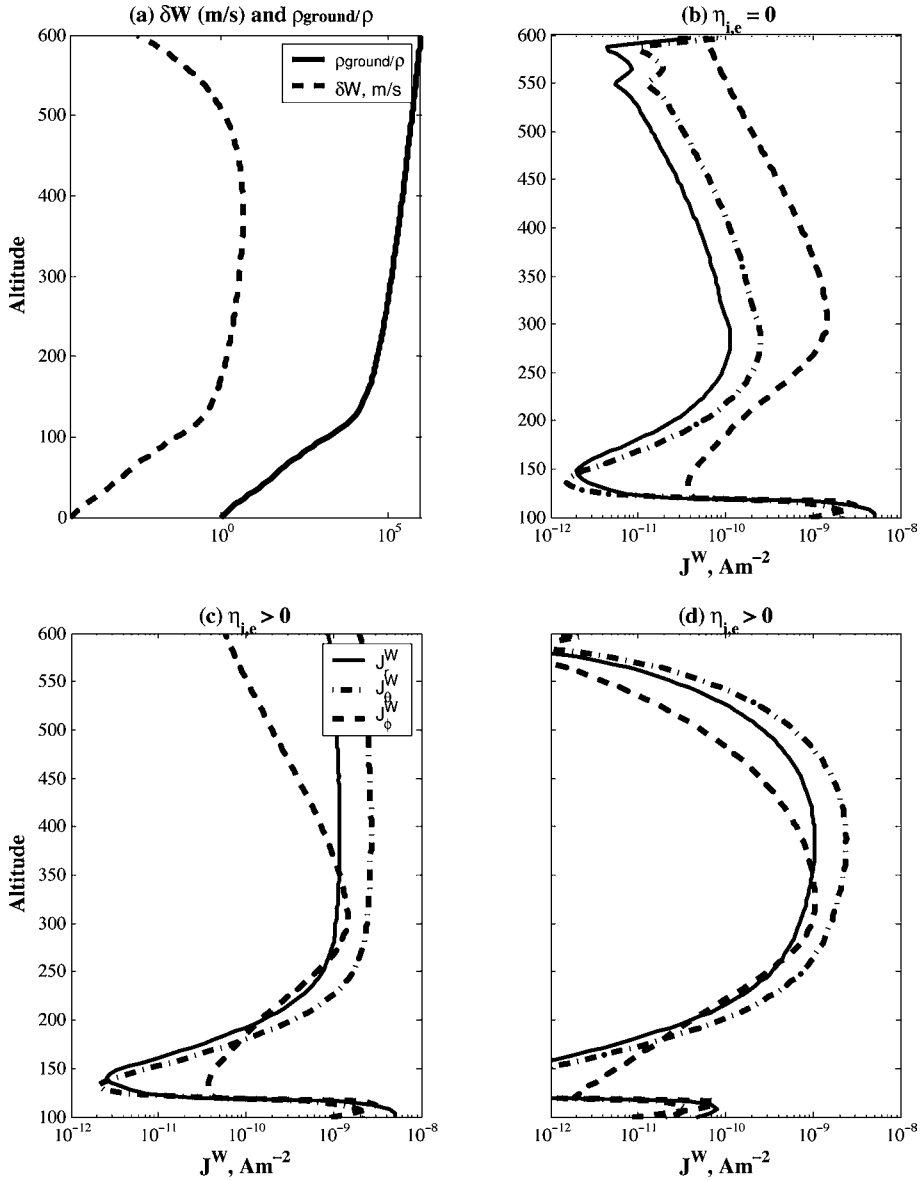

Figure 2. (a) The altitude variations of acoustic wave wind δW and atmospheric amplification factor $\sqrt{\frac{\rho_{\text{ground}}}{\rho(y)}}$, (b and c) the altitude variation of components of current density $\vec{J}^W$ without $\eta_{i,e}$ and with $\eta_{i,e}$, respectively. The currents in (b and c) are summed over latitude and $\delta W_{r,\theta,\phi} = 5\ \text{m s}^{-1}$ is assumed at all altitudes, latitudes and longitudes. (d) The altitude variations of components of (summed) $\vec{J}^W$ with $\eta_{i,e} \neq 0$ and with δW shown in Fig. 2(a).

components $J^W_{r,\theta}$ become significantly different with and without IIA. We note that the large $J^W_{r,\theta}$ flow in the F region due to the IIA and their amplitudes become as large as the J^W_ϕ in the EJ region. Such behaviour indicates that the inertia plays a vital role in determining the current distribution in the ionosphere, particularly in the F region. The $\eta_{i,e}$ dependency of the $J^W_{r,\theta}$ can be explained from the velocity expression (A1) which can be written in the following form, with $\vec{\delta}u'_s$ limited to the part of the current directly related to the wind, expressed by

$$\vec{\delta}u'_s = \underline{\varrho}_s . \delta\vec{W}$$

and which components can be written as:

$$\delta u_s^{\prime r} = \frac{1}{(1+\eta)k_s^2 b^2}\left\{\left[(1+\eta)^2 + \kappa_s^2 b_r^2\right]\delta W_r + \kappa_s^2 b_r b_\theta \delta W_\theta\right\}$$

$$\delta u_s^{\prime\theta} = \frac{1}{(1+\eta)k_s^2 b^2}\left\{\left[(1+\eta)^2 + \kappa_s^2 b_\theta^2\right]\delta W_\theta + \kappa_s^2 b_r b_\theta \delta W_r\right\}$$

$$\delta u_s^{\prime\phi} = \frac{(1+\eta)\kappa}{(1+\eta)\kappa_s^2 b^2}\{b_\theta \delta W_r - b_r \delta W_\theta\}.$$

We note that $\delta u_s^{\prime\phi}$ and thus J^W_ϕ, is independent of η_s as noted in Figs 2(b) and (c). Away from the equator, where $b_r \neq b_\theta \neq 0$, expressions for $\delta u_s^{\prime r,\theta}$ can be simplified to following form:

$$\delta u_s^{\prime r} \approx \frac{b_r}{(1+\eta_s)b}(\hat{b}.\delta\vec{W}); \delta u_s^{\prime\theta} \approx \frac{b_\theta}{(1+\eta_s)b}(\hat{b}.\delta\vec{W})$$
$$\Rightarrow J^W_{r,\theta} \propto \left(\frac{1}{1+\eta_i} - \frac{1}{1+\eta_e}\right)\delta W_\parallel, \quad (14)$$

where $\delta W_\parallel$ is acoustic wave wind parallel to Earth's magnetic field. Thus except at the equator, $J^W_{r,\theta}$ are driven everywhere by parallel

component of δW. However, these currents are significant only when $\eta_{i,e} \neq 0$. Moreover, $J^W_{r,\theta}$ become insignificant in limits $\eta_{i,e} \ll 1$, $\eta_{i,e} \gg 1$. Thus, the contribution of IIA to current is significant only when $\eta_{i,e}$ is smaller than unity but not very small and when difference $\nu_i - \nu_e$ is large. These conditions narrow down the altitude region of maximum IIA contribution to somewhere in between 300 and 500 km.

In Figs 2(b) and (c), the AWs wind, δW, is assumed constant with altitude. This was done to study the effects of $\eta_{i,e}$ variations alone. In reality, δW varies significantly with altitude as shown in Fig. 2(a). One of the objective of this study is to investigate the effects of altitude variations of δW into the ionosphere. To study this aspect, current components, $J^W_{r,\theta,\phi}$, are plotted in Fig. 2(d) for the altitude varying δW shown in Fig. 2(a) and with $\eta_{i,e} \neq 0$. In this figure, we find the similar features as Fig. 2(c) but with more pronounced effect of IIA due to the large δW (Fig. 2a) in the F region and vanishing small perturbation currents in the EJ region due to the small δW (shown in Fig. 2a) in this region. Thus the effect of the altitude varying δW is to rise the large currents in the F region as compared to E region. In Fig. 2(d), the components are summed over latitude and thus the latitude or dip-angle variations do not appear. This is not the case in Figs 3(a)–(c), where the variations of these components (not summed now) with altitude and latitude are shown. The considerable variations with dip-angle of geomagnetic field is noted in these plots despite a uniform δW taken over all latitude.

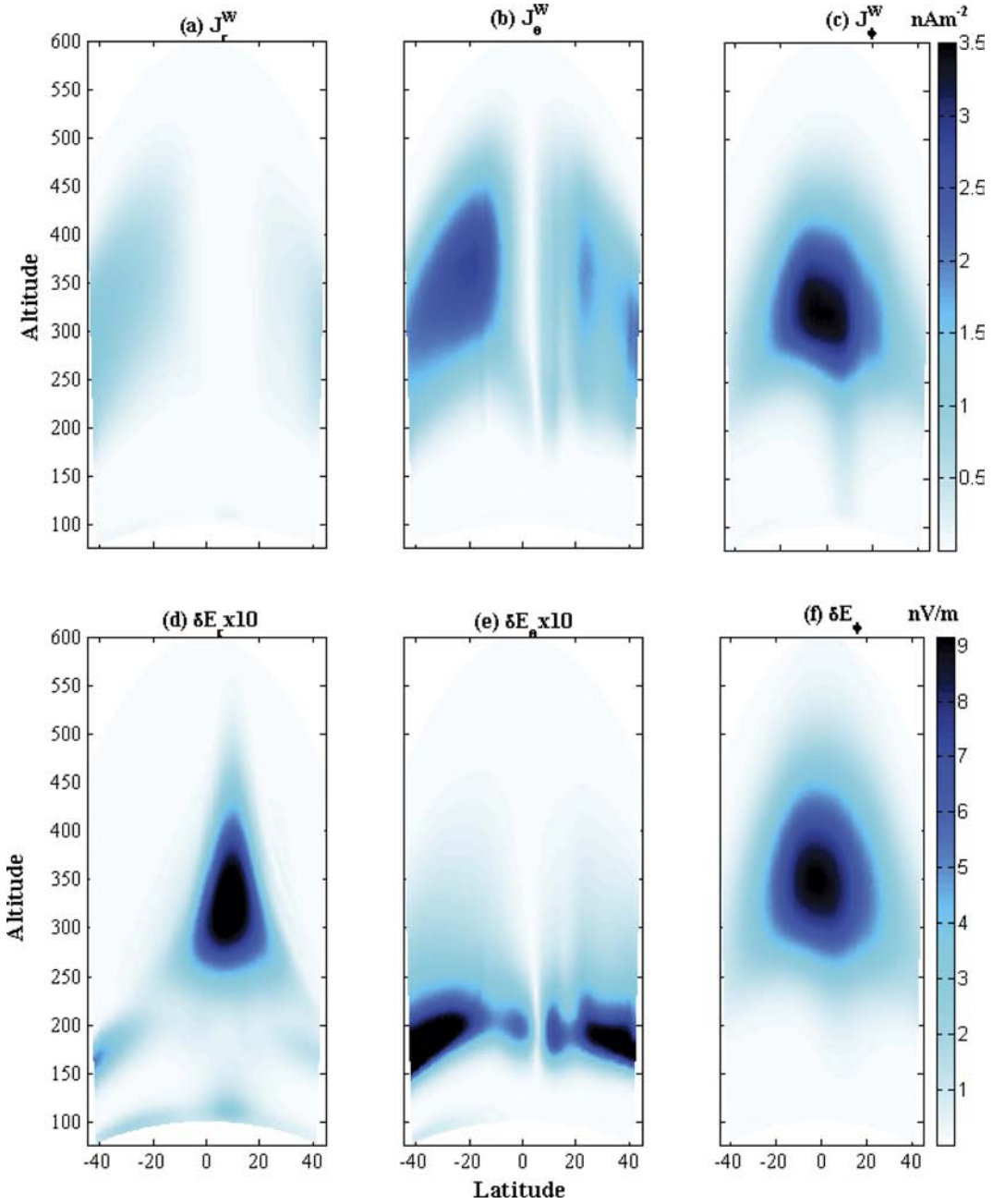

Figure 3. (a–c) The distribution of three components of $\vec{J}^W$ corresponding to δW shown in Fig. 2(a) and (d)–(f) three components of fluctuating electric field $\delta \vec{E}$ (lower panel).

3.3 Electromagnetic and density Fluctuations in the ionosphere

The current distribution shown in Figs 3(a)–(c) includes the effects of $\eta_{i,e}$, altitude variations of δW and dip-angle variations. With such current distribution, the wave eqs (11) and (12) can be solved for $\delta\vec{E}$ and $\delta\vec{B}$. Their components are shown in Figs 3(d)–(f) and 4(a)–(c), respectively. Significant anisotropy and inhomogeneity in these fluctuations are noted. These arise partly due to the inhomogeneous and anisotropic conductivity of the ionosphere and partly due to the variations in AWs wind. The large parallel (to $\vec{B}_o$) conductivity in the F region prevents the excitation of parallel component of $\delta\vec{E}$ in this region. Thus δE_θ which has large parallel components at all latitudes in -40° to 40° range, is excited in the E and lower F region, in spite that the large field-aligned current flows in the F region. This is also true for δE_r component away from the equator. The component δE_r near the equator and δE_ϕ at all latitudes are excited mainly in the F region since they have either no parallel components or very small parallel components. The large parallel conductivity is also responsible for the significant $J^W_{r,\theta}$ and so $\delta J_{r,\theta}$ components in the F region and away from the equator where $\delta W_\parallel \neq 0$. This in turn give rise to large δB_ϕ in this altitude–latitude region. Similarly, in the vicinity of equator, significant J^W_ϕ and so δJ_ϕ gives rise to the dominant $\delta B_{r,\theta}$. We also note that all the three components of $\delta\vec{B}$ are of similar magnitude and δB_ϕ is only large by few factors. We have also found that the spatial distribution and relative magnitudes of components of $\delta\vec{B}$ vary with longitudes and δB_r may become larger than δB_ϕ. We have noted in previous section that in the presence of finite $\delta W_\parallel$, the large current flows in the F region due to the inertia induced acceleration ($\eta_{i,e} \neq 0$). It can be thus said that $\delta W_\parallel$ and $\eta_{i,e} \neq 0$ is essential for the significant current and magnetic field fluctuations in the Ionosphere and particularly in the F region.

The density perturbation $\delta n = n - n_o$, estimated from eq. (10a), is plotted in Fig. 4(d). The considerable altitude and latitude variations are noted in the δn. It is maximum in the F region where $\vec{J}^W$ is large. The maximum $\delta n/n_o$ is found to be 0.01 per cent of ambient density. In addition, the δn is maximum in the vicinity of equator as well as away from the equator. The δn variation is controlled by $\delta\vec{u}$ (eq. 9a) and its divergence. We have found that in the vicinity of equator, the latitude variations of $\delta u_e^{r,\theta}$ are very large (δu_e^r is shown in Fig. 3e) causing the large δn near the equator. Away from the equator, the magnitudes of $\delta u_e^{r,\theta}$ are large due to large $\delta W_\parallel$ (eq. 14) which gives rise to large δn in this latitude region. It can be thus said that similar to electromagnetic fluctuations, the large density perturbation is caused by the large $\delta W_\parallel$. Recently, Rapoport *et al.* (2004) have investigated the 3-D linear response of ionosphere during the passage of the AGWs. They have found that the magnitude of δn depends on the angle between B_o and vertical direction and that the δn tends to be large for large angle. The recent 3-D numerical simulation by Occhipinti *et al.* (2006) has also noted the similar characteristic. From these investigations, it became clear that the AGW's wind component parallel to the $\vec{B}_o$ plays the decisive role in determining δn, that is, large $\delta W_\parallel$ gives rise to large δn. The similar result is found in this investigation.

We should point out that in this investigation, only acoustic channel of AGWs is considered. However, most of the energy of the AGWs resides in the acoustic-gravity channel much below the Brunt-Vaisala frequency. Moreover, the AWs have mainly vertical wind component while the AGWs have both vertical and horizontal components, that is, large $\delta W_\parallel$ at all latitudes. The this investigation thus underestimates the amplitude of fluctuations as compared to the realistic case where complete AGWs spectrum should be considered. Nonetheless, few of the Doppler measurements and GPS TEC fluctuations can be qualitatively discussed here.

Artru *et al.* (2004) have compared the simulated AW's wind fluctuations in the ionosphere and observed ionospheric Doppler velocity fluctuations during few earthquakes and found fairly good agreement between the two. In Figs 4(e) and (f), we present such comparison from this study where radial electron velocity δu_e^r and wind radial component δW_r are plotted. We note that their maximum amplitudes are not very different and found to be in the similar altitude region. However, the latitude distribution is significantly different. On the theoretical ground, we expect the difference between two since the δu_e^r is considerably influenced by Earth's magnetic field. As dip-angle increases, the δu_e^r acquires large component parallel to $\vec{B}_o$, and this component is not affected by $\vec{B}_o$. Thus at large dip-angle, δu_e^r and so the Doppler velocity should become very similar to the δW_r as can be seen from Figs 4(e) and (f). At small dip-angle, the difference between two remains large. Artru *et al.* (2004) have chosen the midlatitude observations in their study. In this latitude region, according to our results, the wind fluctuation and Doppler velocity should be similar as found by them.

Naaman *et al.* (2001) have presented the observations of ionospheric TEC fluctuations for few strong earthquakes. Their study shows that the main contribution to the TEC is from a region with maximum electron density. More recently, 3-D reconstruction of the TEC perturbation during Denali Earthquake (2002 November 03, epicentre: 63.5°N, 147.4°W, $M \sim 7.9$, depth ~4.2 km) also indicate the large density perturbation in the F region (Garcia *et al.* 2005a). Ducic *et al.* (2003) have used the GPS TEC observation to deduce the altitude of maximum coupling during Denali Earthquake and found a maximum correlation at an altitude of 300 k corresponding to the maximum electron density altitude. In this method, one uses GPS data from several different satellites which provide observations over a common area. Each observation is located by the intersection between satellite-receiver ray and the ionospheric layer of altitude 'h'. So for each observation related to a given satellite, we select observations of other satellites which are close up. The horizontal distance between two observations from two different satellites must be lower than d where the parameter d is chosen to be 2 per cent of the wavelength of the post seismic ionospheric perturbation. Consequently, for an altitude 'h' we have a pool of couple of observations matching this rule. Then for each couple we compute coefficient of correlation of the TEC time-series and finally compute the averaged coefficient. Closer the altitude 'h' is to the altitude of the maximum of coupling, higher the averaged coefficient of correlation will be. The Fig. 5 presents the averaged coefficient of correlation for data from satellite 26 and 29 for several altitudes h. We note the maximum correlation or coupling near 300 km altitude which can be taken as the altitude of maximum δn. Thus the GPS observation during Denali Earthquake and other previous observations indicate the maximum δn to be in the F region which is also found in our investigation (Fig. 4d).

3.4 Coupling efficiency between AWs and Ionosphere

Woo & Kahalas (1970) have studied the response of ionosphere during the passage of neutral acoustic waves entering from below. Their 1-D analysis revealed that the excited wave in the ionosphere is an ion-acoustic wave (IAW) and that the coupling efficiency between AWs and IAWs depend on the frequency of AWs and has lower and upper cut-off frequency. The particle flux or wave amplitude

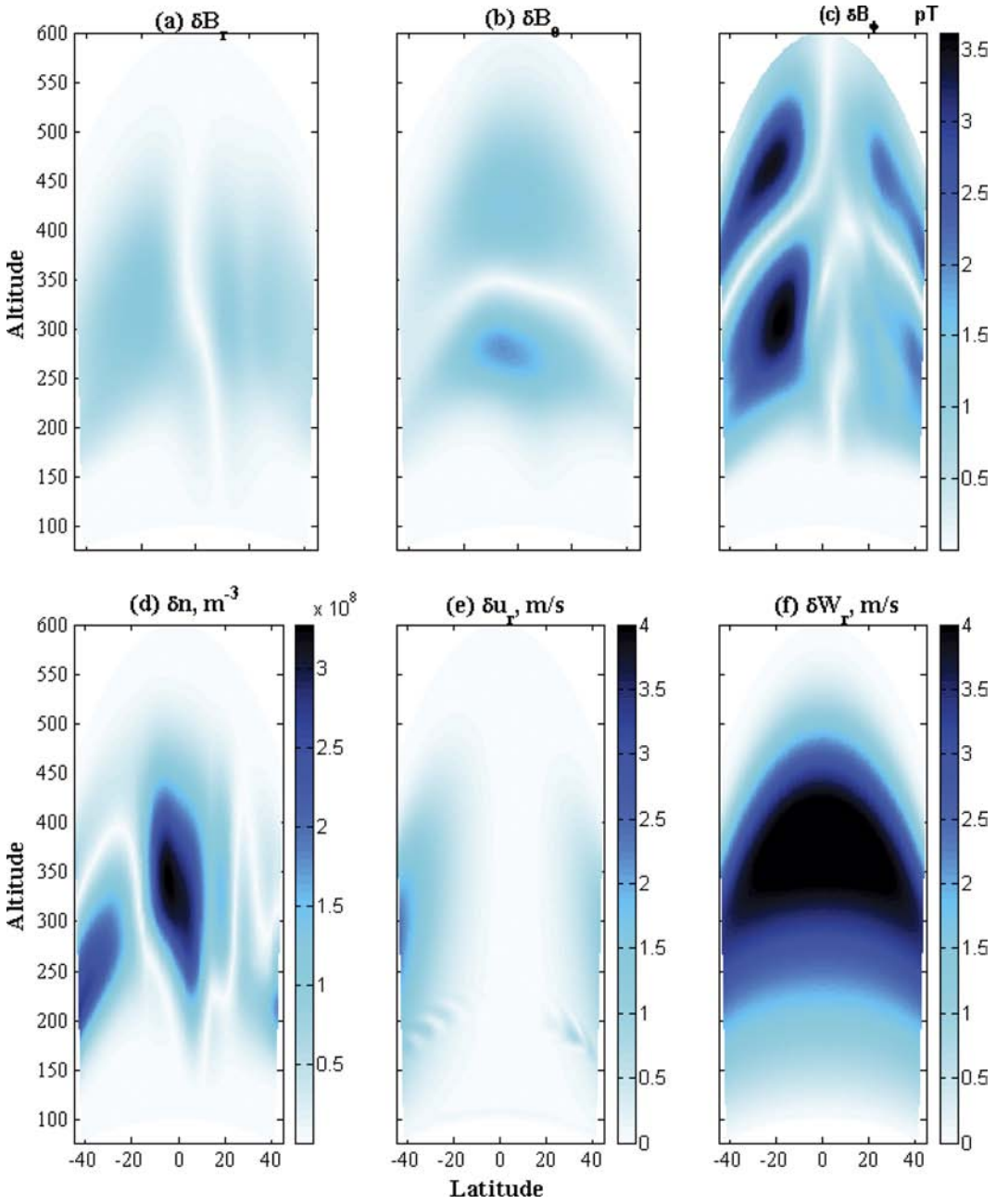

Figure 4. (a–c) The distribution of three components of fluctuating magnetic field $\delta\vec{B}$, (d) density fluctuations δn, (e) perturbed radial velocity of electron δu_e^r and (f) perturbed radial wind δW_r.

was found to be maximum in the range of 0.1–1 Hz. To examine such selective behaviour in this study, we solve eqs (9a, 10a, 11–13) for frequency, $f = \omega/2\pi$, ranging between 10^{-3} and 10 Hz and assuming uniform-isotropic wind $\delta W_{r,\theta,\phi} = 5\ \mathrm{m\,s^{-1}}$ in the ionosphere. The wind is also assumed to be constant with frequency (dash–dotted curve in Fig. 6a). The spectrum of estimated fluctuations ($\delta\vec{J}, \delta\vec{E}, \delta\vec{B}$) are plotted in Figs 6(b)–(d) as dash–dotted curve. In these plots, magnitudes of fluctuations are summed over altitude, latitude and longitudes and then normalized by the total number of bins. We note that the fluctuations are maximum in the 0.1–1 Hz frequency range similar to the result obtained by Woo & Kahalas (1970). As explained by them, this coupling window exists for two reasons: on the lower-frequency side, conditions are not favourable for the excitation of waves in the absence of inertia. As wave frequency increases, the inertia becomes important and waves of significant amplitude are excited provided the AWs find sufficient time to transfer the momentum to ionosphere. This happens for $\omega \sim \nu_i$ and in the 300–500 km altitude region where inertia induced acceleration has significant contribution to the current. In this altitude region, $\nu_{i,e}$ vary in between 1 and 0.1 Hz and thus fluctuations also maximizes in this frequency range. On the higher-frequency side (1–10 Hz), the momentum transfer from AWs to ionosphere becomes insignificant within the time-period of wave (eq. 14) and amplitudes of fluctuations again decreases. As the frequency approaches the ion gyro frequency (~600 Hz), the fluctuations may again grow in amplitude due to the excitation of ion cyclotron waves (Kostarenko *et al.* 1997). In this study, however, such higher frequency range is not studied.

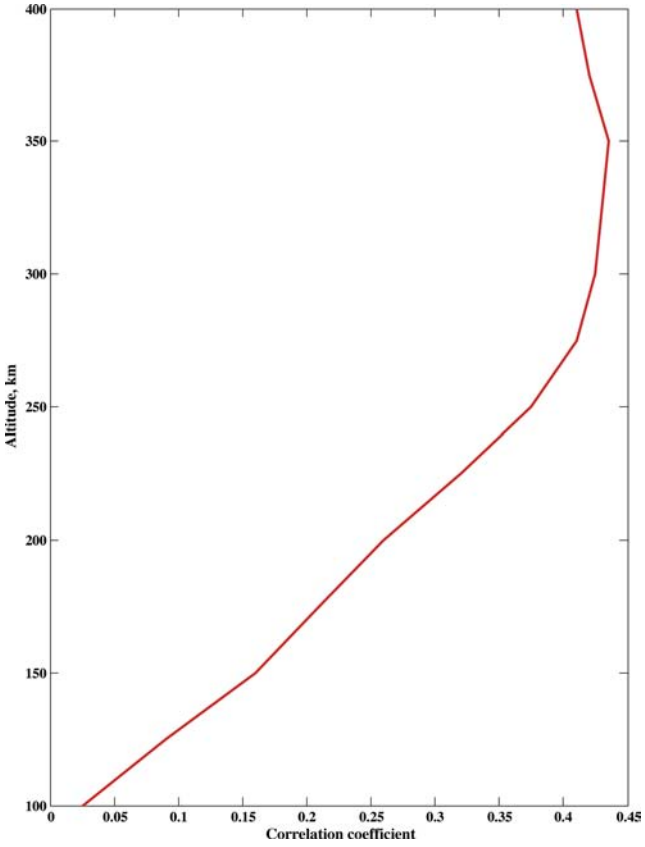

Figure 5. The altitude variation of average correlation coefficient deduced from the GPS observation during Denali earthquake.

It should be pointed out that the presence of Earth's magnetic field in our study does not alter the result obtained by Woo & Kahalas (1970) who had ignored its effects. For the low frequency wave compared to ion-gyro frequency, $\omega \ll \Omega_i$, the important difference which magnetic field brings in this study is to cause the anisotropy in the fluctuations such as noted in Figs 3 and 4. Since, in Figs 6(b)–(d), fluctuations are summed over altitude and latitude, this difference is not seen and the results remain unaltered from Woo & Kahalas (1970). It also means that the excited waves in the ionosphere should be either ion acoustic or slow magneto acoustic waves whose magnitudes (summed over altitude and latitude) would remain unaltered with and without Earth's magnetic field.

While estimating the spectra of the fluctuations in Figs 6(b)–(d), the δW is assumed to be constant over frequency (dash–dotted curve in Fig. 6a). It has been recently shown that only the AWs and AGWs in ULF frequency range (< 0.1 s^{-1}) can reach to the F region heights (Koshevaya *et al.* 2005). Thus δW is expected to vary considerably with frequency in the ionosphere and the spectral features presented above may be modified once this aspect is taken into account. To study this aspect, the spectrum of δW is obtained by solving the 1-D AW model and is plotted in Fig. 6(a) as the solid curve. The δW varies with altitude similar to the Fig. 2(a) for a given frequency though the altitude of maximum amplitude are different for different frequencies. The δW is still assumed to be homogeneous horizontally. The corresponding spectra of fluctuations are plotted in Fig. 6(b)–(d) as the solid curves. It can be seen that the δW maximizes below 0.1 Hz and accordingly the maxima in the fluctuations shift to the lower frequency range below 10^{-2} Hz.

The fluctuations amplitudes discussed so far in Fig. 6, corresponds to the early morning ionospheric conditions. Let us now examine the effects of local time on the amplitude of these fluctuations. In Figs 6(b)–(d), the fluctuations amplitudes are plotted as solid-circle curves for noon-time ionospheric condition. We note that the amplitudes of fluctuations are increased few times from their corresponding early-morning values. Such increase is caused by the increase in the density of ionosphere during noon-time which drives the large current. It can be thus said that for same magnitude of AWs, the coupling between ionosphere and AWs is more efficient during noon (or day-time) than the early-morning or night-time.

While studying the spectral features in Fig. 6, the wind amplitude is assumed to be uniform horizontally. In reality, however, the surface displacement during seismic activity and so the amplitude of AWs vary considerably over Earth's surface (Lognonné *et al.* 1998). To see the effect of horizontally varying δW, two kinds of horizontally varying δW are chosen and they are shown in Fig. 7(a). The δW is still derived from the AWs model and its spectrum is same as solid curve in Fig. 6(a) and it has similar altitude variation as Fig. 2(a). The early-morning ionospheric condition is kept for the estimation. The corresponding spectra of current and electromagnetic fluctuations are plotted in Figs 7(b)–(d). We note that for different horizontally varying δW, the frequency range of maximum coupling remains more or less unaltered but the amplitudes of fluctuations vary significantly.

In Figs 6 and 7, the dominant contribution to the $\delta\vec{J}$, $\delta\vec{E}$ and $\delta\vec{B}$ comes from the F region as noted in Figs 3 and 4. Thus the large current and electro-magnetic fluctuations of μAm^{-2}, nV m^{-1} and nT magnitudes are excited in the F region of ionosphere in the vicinity of 0.01 Hz frequency. These magnitudes are comparable to the magnitudes of current and magnetic field associated with the EEJ region and reveal the importance of F region. The magnetic field fluctuation of nT magnitude in the F region below 1 Hz can be detected from the low-orbiting satellite such as the CHAMP satellite (Balais *et al.* 2005). The satellite orbits near 400 km, covers the frequency range 0.01–1 Hz and has the accuracy of 1–2 nT. On the other side, $\delta\vec{E}$ in this frequency range can be detected from the recently launched DEMETER satellite (Parrot *et al.* 2006), but at an altitude much higher (About 700 km) and probably less optimum. Both satellites might be, therefore, useful to monitor $\delta\vec{E}$ and $\delta\vec{B}$ fluctuations in this frequency range. These measurements are expected to provide the further insight into the nature of ionospheric signatures during a seismic event. More investigations on these measurements and their modelling in the hydromagnetic frame work are needed to understand their nature in the ionosphere.

The fluctuations magnitudes presented in Figs 3 and 4 correspond to the moderate seismic activity of 1 mm surface displacement and early-morning ionospheric condition. For larger seismic event like Sumatra ($M \sim 9$), the surface waves displacement was several cm and the amplitude of the excited AGW has became more than 100 m s^{-1} in the F region (Liu *et al.* 2006a). Such increase in the amplitude of AGW wind should raise the $\vec{J}^W$ to the value of 0.1 μAm^{-2} as compare to 1 n Am^{-2} magnitude in Figs 3(a)–(c). Assuming the noon-time electron density profile, this current can be further raised by few times (as noted in solid-circle curve in Fig. 6b). The electromagnetic fluctuations of nV m^{-1} and nT magnitudes are expected to be excited by current of fraction of μAm^{-2} magnitude. Thus, in the proximity of maximum coupling range, the strong seismic activity

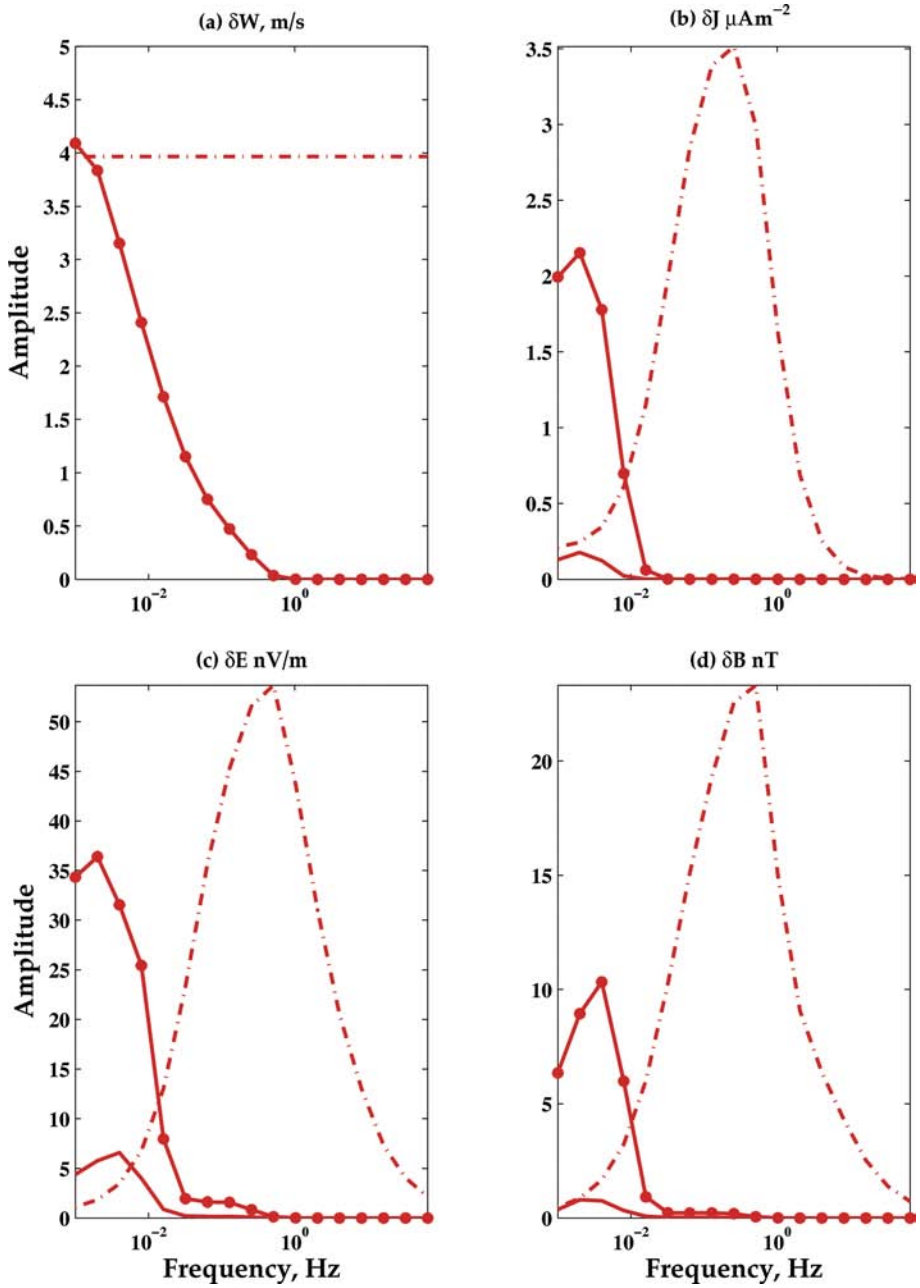

Figure 6. (b–d) The spectrogram of current, electric and magnetic field fluctuations. All the fluctuations are summed over altitude and latitude and divided by number of altitude and latitude bins. The dash curves in (b–d) correspond to the $\delta W_{r,\theta,\phi} = 4$ m s^{-1} (at all altitudes, latitudes, longitudes and frequencies) as shown in (a). The solid and solid-circle curves in (b-d) correspond to the altitude-frequency varying δW shown in Figs 6(a) and 2(a). The solid-circle curves in Figs 6(b)–(d) correspond to the noon-time ionospheric condition.

and particularly the tsunami during noon-time should cause the nV m^{-1} and nT amplitudes of electro-magnetic fluctuations in the F region.

4 SUMMARY AND CONCLUSION

In this investigation, we study the excitation of electromagnetic and density fluctuations in the ionosphere during the passage of seismic triggered acoustic waves. We found that the acoustic waves drive large currents in the F region where their amplitudes and electron density are large. Inertia of ions is found to be essential for driving such large currents. The electromagnetic and density fluctuations excited by such current system are estimated by solving non-local hydromagnetic equations numerically. The fluctuations reveal significant inhomogeneity and anisotropy in space. The electro-magnetic fluctuation is found to be maximum in the F region essentially following the AWs wind driven current system. The density fluctuation also maximizes in the F region. It means that the maximum contribution to the TEC fluctuations from the GPS observation should come from the F region. In addition, all the fluctuations are found to be maximum in the latitude region where wind, $\delta W_{\parallel}$, parallel to Earth's magnetic field $\vec{B}_o$ is large. The $\delta W_{\parallel}$ is thus another essential parameter, apart from the inertia, for large fluctuations in

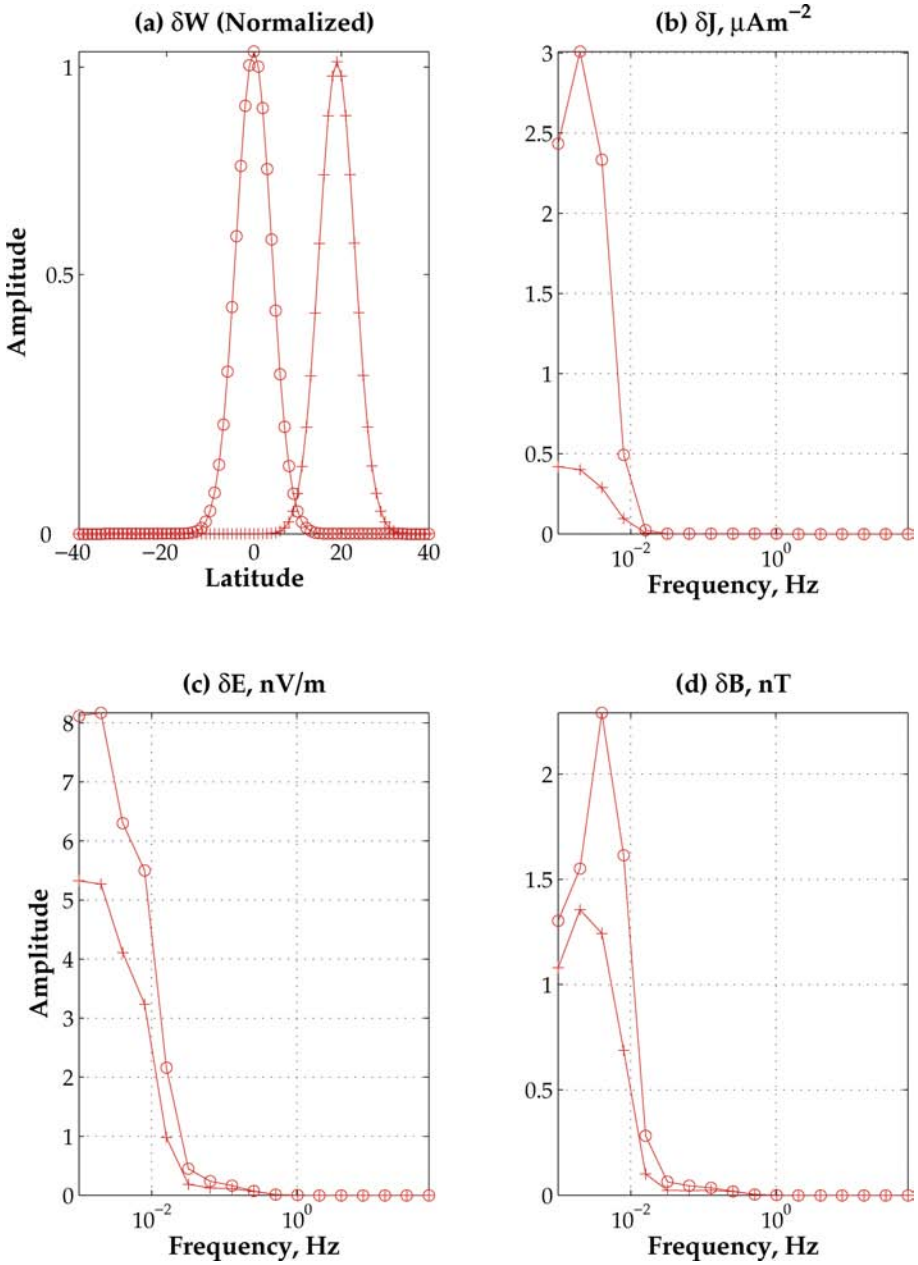

Figure 7. (b–d) The spectrogram of current, electric and magnetic field fluctuations for the horizontally varying δW shown in (a). All the fluctuations are summed over altitude and latitude and divided by number of altitude and latitude bins. The solid-plus and solid-circle curves in (b–d) correspond to the altitude–latitude-frequency varying δW shown in Figs 2(a), 7(a) and 6(a) (solid-circle).

the ionosphere and it is due to the extremely large parallel (to $\vec{B}_o$) conductivity of the ionosphere. Together with the large inertia of ions in the F region, it is exciting significant current and electromagnetic field fluctuations in the F region. The magnitudes of fluctuations are found to be extremely sensitive to the frequency of acoustic waves. The maximum coupling between acoustic waves and ionosphere is noted in 0.1–0.01 Hz. In this frequency range, the magnitudes of current and electro-magnetic fluctuations in F region becomes of order of μAm^{-2}, $nV\,m^{-1}$ and nT. The low-orbiting CHAMP satellite covers this frequency range with an accuracy of nT and capable of detecting these fluctuations. More investigations on the such measurements during a seismic event and their modelling in hydromagnetic framework are needed to understand the nature of electromagnetic fluctuations in the ionosphere. The magnitudes of fluctuations also vary depending on the strength of seismic activity and electron number density. For moderate earthquake during night-time, the magnitudes of current, electric and magnetic fields are found to be of order of nAm^{-2}, $nV\,m^{-1}$ and pT, respectively. For large seismic events and particularly for tsunami during noon-time, the respective amplitudes may reach to nAm^{-2}, $nV\,m^{-1}$ and nT magnitudes.

ACKNOWLEDGMENTS

This work is supported from the ANR CATELL (IONONOMI) and CNES. This is the IPGP contribution number 2373. Authors acknowledge the Naval Research Laboratory for providing SAMI2 model.

REFERENCES

Aburjania, G.D. & Machabeli, G.Z., 1997. New mechanism for electromagnetic field generation by acoustic waves in partial ionized plasmas, *Phys. Lett. A,* **226,** 199–204.

Afraimovich, E.L., Pervalova, N.P., Plotnikov, A.V. & Uralov, A.M., 2001. The shock-acoustic waves generated by earthquakes, *Ann. Geophys.,* **19,** 395–309.

Ahmadov, R.R. & Kunitsyn, V.E., 2004. Simulation of generation and propagation of acoustic gravity waves in the atmosphere during a rocket flight, *Int. J. Geomagnet. Aeron.,* **5,** doi:10.1029/2004GI000064.

Artru, J., Lognonné, P. & Blanc, E., 2001. Normal modes modelling of post-seismic ionospheric oscillations, *Geophys. Res. Lett.,* **28,** 697–700.

Artru, J., Farges, T. & Lognonné, P., 2004. Acoustic waves generated from seismic surface waves:propagation properties determined from Doppler sounding observation and normal-modes modeling, *Geophys. J. Int.,* **158,** 1067–1077.

Artru, J., Ducic, V., Kanamori, H., Lognonné, P. & Murakami, M., 2005. Ionospheric detection of gravity waves induced by tsunamis, *Geophys. J. Int.,* **160,** 840–848.

Balais, G., Maus, S., Luhr, H. & Rother, M., 2005. *Wavelet Analysis of CHAMP Fluxgate Magnetometer Data, Earth Observation with CHAMP*, Springer, New York, 347–352.

Bilitza, D., 2001. International reference ionosphere 2000, *Radio Science,* **36,** 261–275.

Borisov, N.D. & Moiseyev, B.S., 1989. Generation of MHD disturbances in the ionosphere by a Rayleigh wave, *Geomagnet. aeronomy,* **29,** 472–475.

Calais, E. & Minster, B., 1995. GPS detection of ionospheric perturbations following the January 17, 1994, Northridge earthquake, *Geophys. Res. Lett.,* **22,** 1045–1048.

Chmyrev, V.M., Isaev, N.S., Bilichenko, S.V. & stanev, G., 1989. Observation by space-borne detectors pf electric fields and hydromagnetic waves in the ionosphere over the earthquake zone, *Phys. Earth planet Int.,* **57,** 110.

Clévédé, E. & Lognonné, P., 2003. Chapter 85.16, Softwares for: normal modes of the Earth and Planets, in *Handbook on Earthquake and Engineering Seismology*, International Geophysics Series, Vol. 81B, eds Kanamori, H., Jennings, P. & Lee, W., IASPEI Centennial Publications, Academic Press, San Diego.

DasGupta, A., Das, A., Hui, D., Bandhopadhyay, K.K. & Sivaraman, M.R., 2006. Ionospheric perturbations observed by the GPS following the December 2004 Sumatra-Andaman earthquake, *Earth Planets Space,* **58,** 167–172.

Ducic, V., Artru, J. & Lognonné, P., 2003. Ionospheric sensing of the Denali earthquake Rayleigh surface waves, *Geophys. Res. Lett.,* **30,** 1951–1954.

Garcia, R., Crespon, F., Ducic, V. & Lognonné, P., 2005a. 3D ionospheric tomography of post-seismic perturbations produced by the Denali earthquake from GPS data, *Geophys. J. Int.,* **163,** 1049–1064, doi:10.1111/j.1365–246X.2005.02775.x.

Garcia, R., Lognonné, P. & Bonnin, X., 2005b. Detecting atmospheric perturbations produced by Venus quakes, *Geophys. Res. Lett.,* **32,** L16205, doi:10.1029/2005GL023558.

Hao, Y.-Q., Xiao, Z. & Zhang, D.-H., 2006. Response of the ionosphere to the Great Sumatra Earthquake and volcanic eruption of Pinatubo, *Chin. Phys. Lett.,* **23,** 1955.

Hedin, A.E., 1987. MSIS 86 thermospheric model, *J. geophys. Res.,* **92,** 4649.

Hines, C.O., 1960. Internal atmospheric gravity waves, *Can. J. Phys.,* **38,** 1441.

Hobara, Y. & Parrot, M., 2005. Ionospheric perturbations linked to a very powerful seismic event, *J. Atmos. sol. Terre. Phys.,* **67,** 677–685.

Huba, J.D., Joyce & Fedder, J.A., 2000. Sami2 is another model of the ionosphere (SAMI2): A new low-latitude ionosphere model, *J. geophys. Res.,* **105,** 23035–23053.

Jacobson, A.R. & Bernhardt, P.A., 1985. electrostatic effects in the coupling of upper atmospheric waves to ionospheric plasma, *J. geophys. Res.,* **90,** 6533–6541.

Kelley, M.C., 1989. *The Earth's Ionosphere, Plasma Physics and Electrodynamics*, Academic Press, San Diego, CA., (**43**).

Kherani, E.A., de Paula, E.R. & Bertoni, F.C.P., 2004. Effects of the fringe field of Rayleigh-Taylor instability in the equatorial E and valley regions, *J. geophys. Res.,* **109,** A12310, doi:10.1029/2003JA010364.

Kherani, E.A., Mascarenhas, M., Sobral, J.H.A., de Paula, E.R. & Bertoni, F.C., 2005. A three dimension simulation model of collisional interchange instability, *Space Sci. Rev.,* **121,** 253–269.

Koshevaya, S., Makarets, N., Grimalsky, V., Kostarenko, A. & Perez Enriques, R., 2005. Spectrum of the seismic-electromagnetic and acoustic waves caused by seismic and volcano activity, *Nat. Hazards Earth Syst. Sci.,* **5,** 203–209.

Kostarenko, N.Y., Enriquez, R.P. & Koshewaya, S.V., 1997. Excitation of plasma waves in the ionosphere caused by atmospheric gravity waves, *Astrophys. Space Sci.,* **246,** 211–217.

Liu, J.Y., Tsai, Y.B., Chen, S.W., Lee, C.P., Chen, Y.C., Yen, H.Y., Chang, W.Y. & Liu, C., 2006a. Giant ionospheric distrubances excited by the M9.3 Sumatra earthquake of 26 December 2004, *Geophys. Res. Lett.,* **33,** L02103.

Liu, J., Tsai, Y., Ma, K., Chen, Y., Tsai, H., Lin, C., Kamogawa, M. & Lee, C., 2006b. Ionospheric GPS total electron content (TEC) disturbances triggered by the 26 December 2004 Indian Ocean tsunami, *J. geophys. Res.,* **111,** A05303.

Lognonné, P. & Clévédé, E., 2002. Chapter 10: normal modes of the Earth and Planets, in *Handbook on Earthquake and Engineering Seismology*, International Geophysics Series, Vol. 81A, pp. 125–147, eds Kanamori, H., Jennings, P. & Lee, W., IASPEI Centennial Publications, Academic Press, San Diego.

Lognonné, P., Clévédé, E. & Kanamori, H., 1998. Computation of seismograms and atmospheric oscillations by normal-mode summation for a spherical earth model with realistic atmosphere, *Geophys. J. Int.,* **138,** 388–406.

Lognonné, P. *et al.*, 2006. Ground-based GPS imaging of ionosphere post-seismic signal, *Planet. Space Sci.,* **54,** 528–540.

Naaman, Sh., Alperovish, L.S., Wdowinski, Sh., Hayakawa, M. & Calais, E., 2001. Comparison of simultaneous variations of the ionospheric total electron content and geomagnetic field associated with strong earthquakes, *Nat. Hazards Earth Syst. Sci.,* **1,** 53–59.

Occhipinti, G., Lognonné, P., Kherani, E.A. & Hebert, H., 2006. Three-dimensional waveform modeling of ionospheric signature induced by the 2004 Sumatra tsunami, *Geophys. Res. Lett.,* **33,** L20104.

Occhipinti, G., Kherani, E.A. & Lognonné, P., 2008. Geomagnetic dependence of ionospheric disturbances induced by tsunamigenic internal gravity waves, *Geophys. J. Int.,* **173,** 753–765.

Parks, G.K., 2004. *Physics of Space Plasmas, An Introduction*, Westward Publication, pp. 80–90.

Parrot, M., Berthelier, J.J., Lebreton, J.P., Sauvaud, J.A., Santolik, O. & Blecki, J., 2005. Examples of unusal ionospheric observations from the DEMETER satellite over seismic regions, *Phys. Chem. Earth,* **31,** 486–495.

Pokhotelov, O., Parrot, M., Fedorov, E., Pilipenko, V., Surkov, V. & Gladychev, V., 1995. Response of the ionosphere to natural and man-made acoustic sources, *Ann. Geophys.,* **13,** 1197–1210.

Rapoport, Yu.G., Gotynyan, O.E., Ivchenko, V.M., Kozak, L.V. & Parrot, M., 2004. Effect of acoutic gravity wave of the lithospheric origin on the ionospheric F region before earthquakes, *Phys. Chem. Earth,* **29,** 607–616.

Sorokin, V.M., Yaschenko, A.K. & Hayakawa, M., 2006. Formation mechanism of the lower-ionospheric disturbances by the atmosphere electric current over a seismic region, *J. Atmos. Sol. Terr. Phys.,* **68,** 1260–1268.

Surukov, V.V., 1992. Excitation of low-frequency geomagnetic oscillations upon the propagation of a vertical acoustic waves in the E layer of the ionosphere, *Geomagnet. Aeronomy,* **32,** 332–335.

Woo, C.J. & Kahalas, S.L., 1970. Collisionnal coupling of Neutral-to plasma Acoustic waves in a diffuse layer, *Phys. Fluids,* **13,** 712–720.

Yuen, P.C., Weaver, P.F., Suzuki, R.K. & Furumoto, A.S., 1969. Continuous travelling coupling between seismic waves and the ionosphere evident in Earth, *J. geophys. Res.,* **96,** 20 309–20 319.

APPENDIX A

In spherical polar coordinate, eq. (9) can be written in following matrix form:

$$\begin{pmatrix} u_r \\ u_\theta \\ u_\varphi \end{pmatrix} = \underline{\varrho}. \begin{bmatrix} \zeta_s E_r + W_r - \frac{c_s^2}{n_o}(\nabla \delta n)_r \\ \zeta_s E_\theta + W_\theta - \frac{c_s^2}{n_o}(\nabla \delta n)_\theta \\ \zeta_s E_\varphi + W_\varphi - \frac{c_s^2}{n_o}(\nabla \delta n)_\phi \end{bmatrix}, \tag{A1}$$

where $\underline{\varrho}$ is the mobility tensor given by:

$$\underline{\varrho} = \begin{pmatrix} 1+\eta_s & -\kappa_a b_\varphi & \kappa_s b_\theta \\ \kappa_a b_\varphi & 1+\eta_s & -\kappa_s b_r \\ -\kappa_s b_\theta & \kappa_s b_r & 1+\eta_s \end{pmatrix}^{-1}$$

and $\eta_s = \frac{i\omega}{\nu_s}$, $\zeta_s = \frac{q_s}{m_s \nu_s}$, $(b_r,\ b_\theta,\ b_\phi)$ are the unit vector components of Earth's magnetic field. The conductivity tensor $\underline{\sigma}$ in eq (6) is defined as:

$$\underline{\sigma} = n_o e(\varrho_i \zeta_i - \varrho_e \zeta_e).$$